Volume 1 | Number 1 | Jan 2013 | Pages 1–100

Nanoscale

www.rsc.org/nanoscale

ROYAL SOCIETY OF CHEMISTRY

ROYAL SOCIETY OF CHEMISTRY

www.rsc.org/nanoscale

Nanoscale

ARTICLE TYPE

Designing Multicolor Long Range Nanoscopic Ruler for Imaging of Heterogeneous Tumor Cells

Suhash Reddy Chavva , Bhanu Priya Viraka Nellore, Avijit Pramanik, Sudarson Sekhar Sinha,
Stacy Jones and Paresh Chandra Ray *

Tumor heterogeneity is one of the biggest challenges in cancer treatment and diagnosis. Multicolor optical ruler is essential to address heterogeneous tumor cells complexity. Driven by the need, current article reports the design of multicolor long range nanoscopic ruler for screening tumor heterogeneity by accurately identifying epithelial cells and cancer stem cells (CSCs) simultaneously. Nanoscopic surface energy transfer (NSET) ruler has been developed using blue fluorescence polymer dots (PDs) and red fluorescence gold cluster dots (GCDs) as multicolor fluorescence donor and plasmonic gold nanoparticle (GNP) acts as an excellent acceptor. Reported experimental results demonstrated that the multicolor nanoscopic ruler's working window is above 35 nm distances, which is more than three times farther than that of Förster resonance energy transfer (FRET) distance limit. Theoretical modeling using Förster dipole−dipole coupling and dipole to nanoparticle surface energy transfer have been used to discuss the possible mechanism for multicolor nanoscopic ruler's long-range capability. Using RNA aptamer that are specific for the target cancer cells, experimental data demonstrate that nanoscopic ruler can be used for screening epithelial and CSCs simultaneously from whole blood sample with 10 Cells/mL detection capability. Experimental data show that nanoscopic ruler can distinguish targeted cells from non-targeted cells.

Introduction

Despite the huge advances in cancer treatment and diagnosis, due to the tumor heterogeneity, cancer is the second leading cause of death for human being in our world [1-4]. Conventional therapies are often failure due to the persistence of cancer stem cells (CSCs) with cancer epithelial cells in tumor environment [4-7]. CSCs are heterogeneous subpopulation of rare cells within cancer tumors, which exhibits extensive self-renewal and they account for tumor growth, invasion and metastasis [8-10]. Several recent studies have demonstrated that during epithelial-mesenchymal transition (EMT), some epithelial cells are transformed into CSCs [4-8], as shown in Scheme 1. As a result, blood sample in cancer patients will contain cancer epithelial cells and cancer stem cells together.

Department of Chemistry and Biochemistry, Jackson State University, Jackson, MS, USA; E-mail:paresh.c.ray@jsums.edu; Fax:+16019793674.
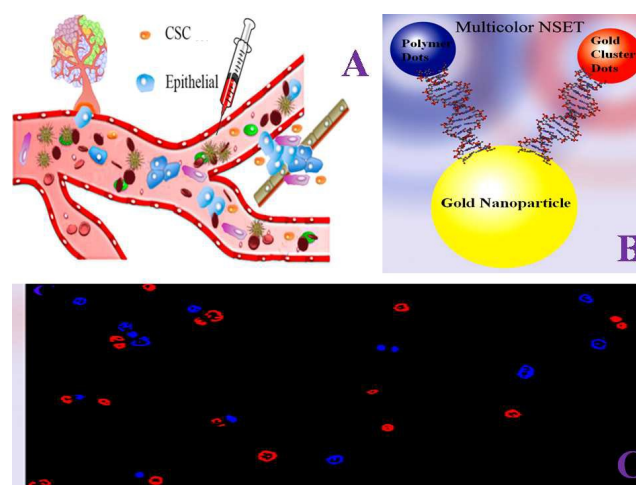
Scheme 1: A) Schematic representation shows the heterogeneous nature of tumor cells in blood containing epithelial and cancer stem cells. B) Schematic representation showing the development of multicolor NSET ruler using blue fluorescence polymer dots (PDs) and red fluorescence gold cluster dots (GCDs) as multicolor fluorescence donor and plasmonic gold nanoparticle (GNP) acts as an excellent acceptor. C) Multicolor fluorescence imaging shows tumor heterogeneity identification capability using multicolor NSET ruler.

Recent clinical trials results indicate that identifying CSCs and epithelial cancer cells in the blood can be used as a non-invasive diagnostic procedure for screening patients who may be at high risk for developing metastatic or relapse of cancer [1,3]. Since for the complete understanding of complex cancer heterogeneity, multi-color detection capability is essential, here we reports the development of long-range two color nanoscopic ruler, as shown in Scheme 1A. In our multicolor nanoscpic ruler design, blue fluorescence polymer dots (PDs)) and red fluorescence gold cluster dots (GCDs) act as a donor and plasmonic gold nanoparticle acts as a acceptor, as shown in Scheme 1. Multicolor fluorescence nanodots are separated from plasmnic GNP by bi-functional rigid double strand RNA molecule, which controls the multicolor nanoscopic ruler length.
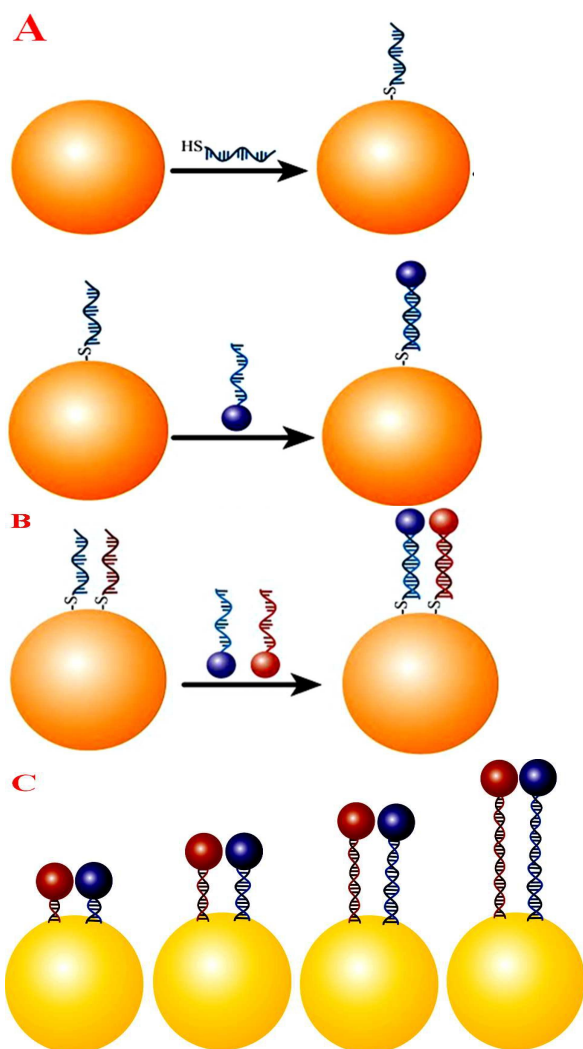
Figure 1: Schematic representation illustrates A) Synthetic method for developing a blue color fluorescence PD based nanoscopic ruler using gold nanoparticle as a quencher. ds-RNA has been used to couple donor and acceptor. B) Synthetic method for developing multicolor nanoscopic ruler using blue color fluorescence polymerdots and red color fluorescence gold dots. Gold nanoparticle has been used as a acceptor and ds-DNA has been used to couple the donor and the acceptor. C) The design of multicolor nanoscopic ruler using different length ds-RNA.

In last one decade considerable efforts have been devoted in the development of nanoscopic surface energy transfer (NSET) ruler to expand the range of the biophysical toolset beyond Förster resonance energy transfer (FRET) spectroscopy ruler [9,11-16]. Last few years, due to very good photostability and bio-compatibility, polymer dots (PDs) and gold cluster dots (GCDs) have emerged as bright fluorescence imaging probes [17-29]. Since the nanoparticles have huge surface area, it allows chemical conjugation of multiple acceptors like polymer dots and gold dots together onto its surface. Due to the huge surface area and extremely high extinction coefficient, each metal nanoparticle can be used as an optical probe equivalent to several million dye molecules[11-15]. Reported data shows that the multicolor nanoparticle surface energy transfer (NSET) ruler's distance

window can be extended more than 30 nm distance, which is more than three times that of well recognized FRET optical ruler. To demonstrate the utility of the multicolor nanoscopic ruler for multiplex detection, we have developed multicolor NSET by using DNA/RNA aptamer that are specific for the target cancer cells. One side of the aptamer is attached with fluorescence nanodot which acts as a donor and other side of the aptamer is attached with plasmonic gold nanoparticle, which acts as an acceptor or a quencher. Reported data indicate that the aptamer based multicolor NSET ruler can be used for screening epithelial, and cancer stem cells (CSCs) selectively and simultaneously with 10 cells/mL detection capability.

Results and Discussions

We have designed a long range multicolor nanoscopic ruler r from 2 to 35 nm range using SH-modified dsDNA as a coupling agent between fluorescence nanodots and plasmonic gold nanoparticle. Since the interaction between GNPs and DNA can cause the ds-DNA to be bend[24], we have used 100−120 DNA/nanoparticle surface to minimize the bending of the dsDNA. Recently it has been reported that more the DNA molecule bonds to the surface, the lesser is the probability of bending[24]. Spherical gold nanoparticles of around 40 nm size were synthesized by using gold chloride ($HAuCl_4$, $3H_2O$) and sodium citrate, using citrate reduction method as we have reported before [11,13,14]. Details of the synthesis and characterizations have been reported in the experimental section. We have developed blue fluorescent polymer dots (PDs) using amphiphilic polymer solvent evaporation technique[17]. Synthesis details and characterizations have been reported in the experimental section. Figure 2C shows the fluorescence from freshly prepared PD. The photoluminescence quantum yield (QY) for PD was determined to be 0.69 at 380 nm light excitation, using quinine sulfate as a standard (QY 54%). Red fluorescent GCD nanoprobes capped with a bidentate ligand, dihydrolipoic acid (DHLA) were developed by mixing sodium hydroxide, α-lipoic acid, $HAuCl_4.3H_2O$ and $NaBH_4$ with constant stirring [29]. Synthesis and characterization details have been reported in the experimental section. Figure 2A shows the fluorescence from freshly prepared GCD. The photoluminescence quantum yield (QY) for GCD was determined to be 0.13 at 380 nm light excitation, using quinine sulfate as a standard (QY 54%).

To design long-range multicolor NSET optical rulers of different lengths, we used 5′-PD/GCS- and 3′-SH modified ssRNA of different lengths. After hybridization with complementary oligonucleotides, the separation distances between the GNP and PD/GCD nanodots were systematically varied. For this purpose, we have used the captured oligonucleotides from 2 mer to 130 mer. Some of the oligonucleotides structure are shown in supporting information. To design the long range NSET ruler, we first developed PD modified oligonucleotides at different length, which is complimentary of captured oligonucleotide. For this purpose we have used amine modified oligonucleotides for labeling with blue polymer dots. For the formation of blue color fluorescent PD labeled oligonucleotides, we have used EDC/NHS esterification for the conjugation between amine group of amine modified aptamer and -OH group of polymer dots. Similarly for the development of GCD modified oligonucleotides at different length, we have used coupling chemistry between -CO_2H group of α-lipoic acid attached GCDs and -NH_2 group of amine-functionalized oligonucleotides via amide linkages in the presence of 1-(3-dimethyl-aminopropyl)-3-ethylcarbodiimide

hydrochloride (EDC). In the next step, 3′- SH-modified ssRNA was attached to GNPs via thiol-gold chemistry, as shown in Figure 1A-B.
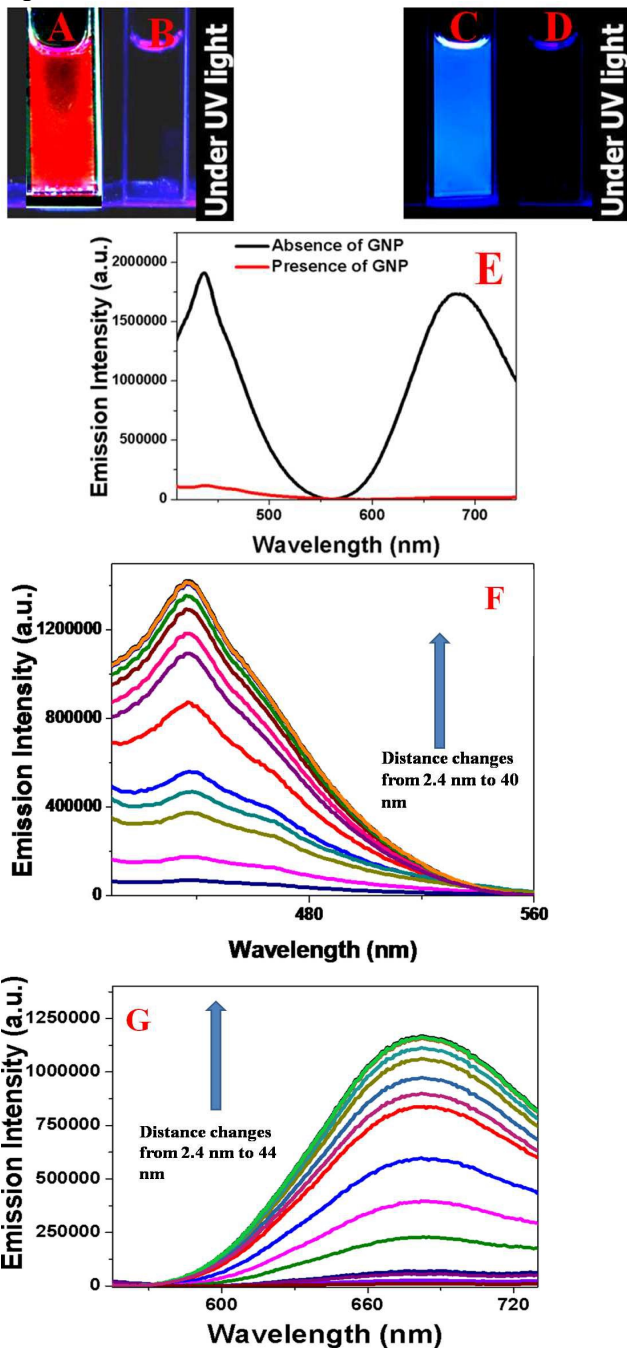

Figure 2: A, B) Fluorescence image under UV light; A: red fluorescence from GCD. B: Fluorescence disappears when it attached with GNP using 6 mer RNA. C: blue fluorescence from PD. D: Fluorescence disappears when it attached with GNP using 6 mer RNA. D) Fluorescence spectra from the mixture of PD coated Apt. 1 aptamer and GCD coated S6 aptamer in the presence and absence of gold nanoparticle , F) Variation of fluorescence intensity for optical rulers with the increase in distance between PD and GNP using dsRNAs of different lengths (2-108 mer). G) Variation of fluorescence intensity for optical rulers with the increase in distance between GCD and GNP using dsRNAs of different lengths (2-130 mer).

After that, hybridization was performed using a PD/GCD coated complementary sequences attached gold nanoparticles in 10 mM PBS solution containing 0.3 M NaCl. To make sure that the hybridization was almost complete, we used a 1:10 ratio of probe-to-target sequence. Excess PD/GCD coated complementary ssRNA, which were not involved in hybridization were removed by centrifugation from the solution. In our design, we used dsDNA spacers of 2 to 130 base pairs to design spectroscopy ruler window from 3 to 44.4 nm.

In our design, we have estimated the "multicolor NSET ruler" distance using the simple model reported by Clegg et al. [30], by taking into account the size of the 0.32 nm for each base pair. We have also used 2.8 nm for Au–S-$(CH_2)_n$-RNA and RNA-PD distance in both sides of base pair. To find out the validity of the rigid-rod approximation, we have also measured the NSET rular distance using dynamic light scattering (DLS), as reported in Table 1. DLS data match very well with the calculated data. Figure 2C shows the variation of quenching efficiency with increasing the distance between 40 GNP and PD. Similarly, Figure 2D shows the variation of quenching efficiency with increasing the distance between 40 GNP and GCD.

Table 1: NSET ruler distance measured by dynamic light scattering technique and calculated using rigid-rod approximation.

NSET ruler description	Distance measured by DLS	Calculated distance
GNP and PD separated by ds-2bp RNA	2.4 ± .2 nm	2.44 nm
GNP and PD separated by ds-10bp RNA	6.2 ± .4 nm	6.0 nm
GNP and PD separated by ds-30bp RNA	12.5 ± .8 nm	12.4 nm
GNP and PD separated by ds-60bp RNA	22.0 ± 1.0 nm	22.0 nm
GNP and PD separated by ds-90bp RNA	32.0 ± 1.5 nm	31.6 nm
GNP and PD separated by ds-110bp RNA	37.0 ± 2 nm	38 nm
GNP and PD separated by ds-130bp RNA	45.0 ± 3 nm	44.4 nm

The quenching efficiency was determined by comparison against control PD/GCD attached D-ds-RNA in the absence of 40 nm gold nanoparticle, using the following equation [12,15]:

$$Q_{ruler} = 1 - \frac{I_{ruler} A_{control}}{I_{control} A_{ruler}} \qquad (1)$$

where Q_{ruler} is the quenching efficiency due to energy transfer between PD/GCD and gold nanoparticle via NSET. We have find out the I_{ruler} and $I_{control}$ using the integrated intensities under the curve for the emission peak due to the ruler and control. A_{ruler} and $A_{control}$ are the absorption values of the ruler and control at the peak of the PD/GCD. As reported in Figures 2C and 2D, experimental data clearly indicate that NSET ruler based on 40 nm gold nanoparticle as a quencher and PD/GCD as a donor, the ruler is highly sensitive to small changes in the PD/GCD−GNP distance even if they are separated for more than 35 nm, which is 3.5 times larger than the FRET distance limit. Figure 2C and 2D clearly indicate that when the ruler distance is between 3-6 nm, about 95% fluorescence from PD/GCD nanodots is quenched by 40 nm gold nanoparticle. It is due to the fact that, due to the huge 2-D surface, large molar extinction coefficients ($\sim 10^5$ cm^{-1} M^{-1}) and extremely high Stern–Volmer constants (K_{SV}), gold nanoparticles acts as a super quencher[11-15]. As a result, bright fluorescence from nanodots is completely quenched when PDs and GCDs were within 6 nm from the particle surface. Since the

nanoparticles have huge surface area, it allows chemical conjugation of multiple acceptors like polymer dots and gold dots together onto its surface. Gold nanoparticles are known as highly efficient energy acceptors, as a result, it has been used as acceptor to design NSET probe [9,11-16]. When an acceptor gold nanoparticle and a donor nanodots are brought into proximity using –ds DNA, there is a dipole-surface type energy transfer from nanodots dipole to gold nanomaterial nanometal surface, which can be termed as nanoparticle based surface energy transfer (NSET)[11-15]. Since in case of NSET, acceptor gold nanoparticle has a surface with isotropic distribution of dipole vectors to accept energy from the fluorescent nanodots donor, NSET does not require a resonant electronic transitions like FRET. Also due to the huge surface area and extremely high extinction coefficient, each gold nanoparticle can be used as an optical probe equivalent to several million dye molecules[11-15]. Due to the above facts, single gold nanoparticle can acts as an acceptor for several multicolor nanodots simultaneously.

To find out the distant dependent quenching process between 40 nm GNP and PD/GCD fluorescence nanodots, we have employed theoretical modeling using Förster dipole−dipole coupling and NSET based dipole-to NSET as reported by Jenning et al. In case of FRET, the quantum efficiency of energy transfer can be written as[11-15]

$$\Phi_{FRET} = \cfrac{1}{1+\left(\cfrac{R}{R_0}\right)^6} \qquad (2)$$

where R is the distance between organic dye donor and organic acceptor and R_0 is the distance between donor and acceptor at which the energy transfer efficiency is 50% . Our experimental data as reported in Figure 3A clearly show that the long distance quenching rate cannot be discussed using the classical $1/R^6$ characteristic of FRET. Rather than one has to describe it using a slower distance-dependent quenching rate. Due to the involvement of several parameters like surface charge, surface coverage, incident laser light polarizations, absorption and scattering cross-section of GNPs, plasmonic overlap between GNP and possible donors, the interactions between GNP and PD/GCD are quite complex. As a result, Förster dipole−dipole coupling FRET, which physically originates from the weak electromagnetic coupling of two dipoles will not be able explain the slower distance-dependent quenching rate, which clearly indicates that one has to use more coupling interactions to circumvent the FRET limit. In case of NSET, where a point dipole interacting with an infinite metal surface, as proposed by Strouse and co-workers[12,15], the energy transfer efficiency can be written as

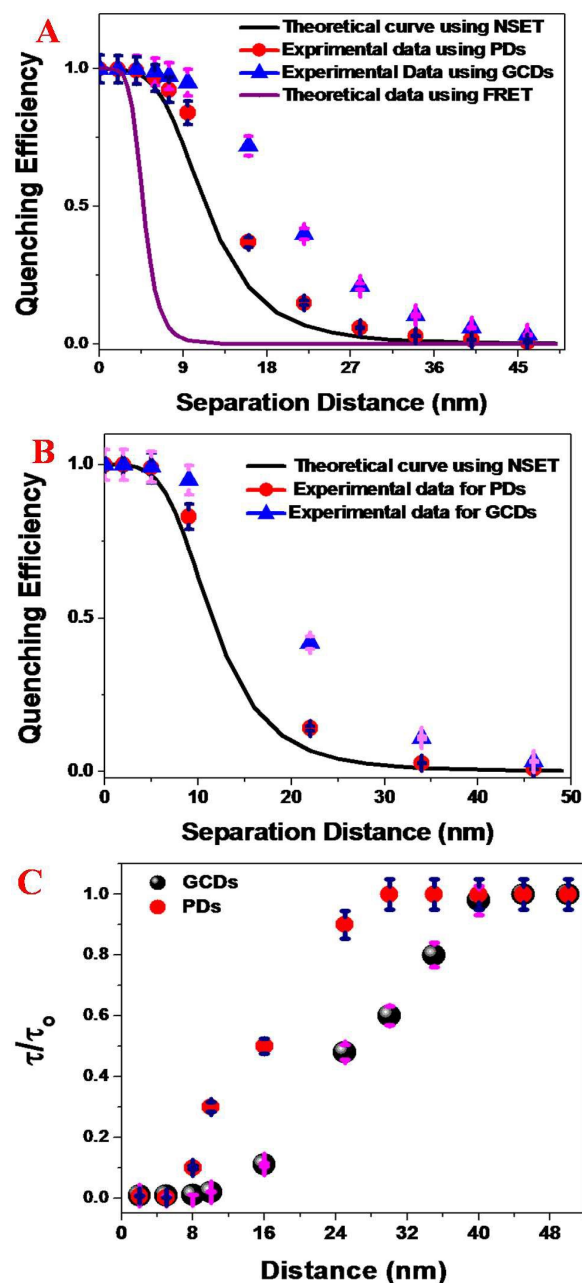$$E = \cfrac{1}{1+\left(\cfrac{R}{R_0}\right)^4} \qquad (3)$$

R_0, which is the distance between donor and acceptor at which the energy transfer efficiency is 50% can be defined as,
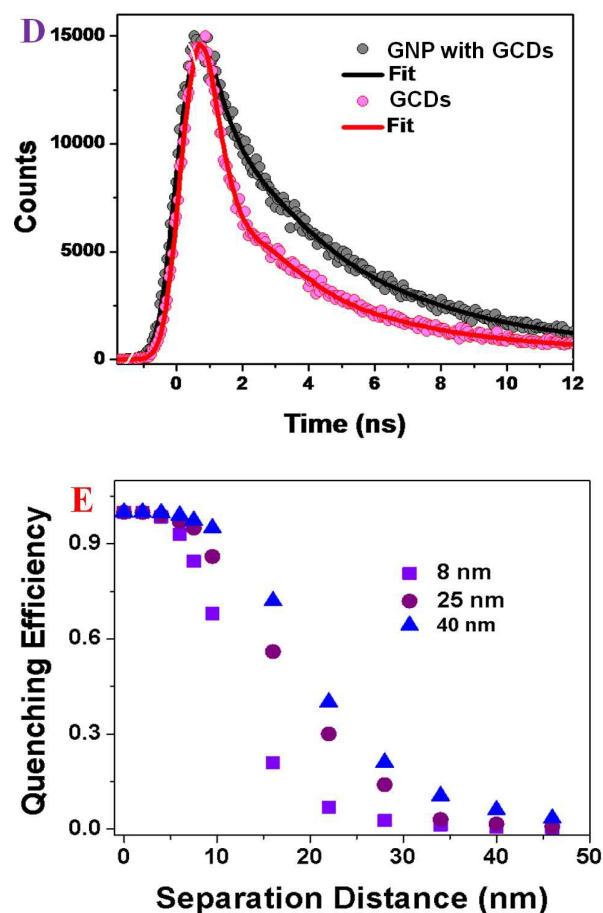
$$R_0 = \frac{\alpha\lambda}{n_m}\left(A\phi\right)^{1/4}\left[\frac{n_r}{2n_m}\left(1+\frac{\varepsilon_1^2}{|\varepsilon_2|^2}\right)\right]^{1/4} \qquad (4)$$

Where λ is the emission wavelength maximum for the donor and ϕ the quantum yield of the donor. ε_1 is the dielectric

constant of the solvent. n_m is refractive index of solvent. The orientation factor of the donor to the metal plasmon vector is α .

A is the absorptivity or extinction coefficient of thin film mirror. Experimental data as reported in Figure 3A shows a good agreement with NSET model for polymer dots as donor and GNP as acceptor. On the other hand, the agreement is quite poor with NSET model when gold cluster dots acts as donor and GNP acts as an acceptor. Quenching efficiency is also highly dependent on the excited-state donor lifetime, as we and others have discussed before [11-15]. At small distances, the quenching efficiency is dependent on the nonradiative rate, whereas at higher distance, the distance dependent quantum efficiency is almost exclusively governed by the radiative rate[11-15].

Figure 3 A): Variation of quenching efficiency with the distance between 40 nm GNPs and fluorescence nanodots for single color NSET ruler. Plot also shows theoretical fitting data for the variation of the quenching efficiency with distance using the FRET and NSET formula. B) Variation of quenching efficiency with the distance between 40 nm GNPs and fluorescence nanodots for multi color NSET ruler. Plot also shows theoretical fitting data for the variation of the quenching efficiency with distance using the NSET formula. C) Distance dependent fluorescence lifetime τ for PD/GCD, which is normalized to the fluorescence lifetime τ_0 in the absence of gold nanoparticle. D) Life-time decay of fluorescence from GCDS and gold nanoparticle attached GCDs via –ds RNA. E) Plots shows the distance-dependent quenching efficiency between GCDs and GNP is highly dependent on the gold particle size.

Figure 3D shows the lifetime decay for GCD and GNP conjugated GCD. The fluorescent lifetime was determined using Horiba Jobin Yvon fluorolog instrument attached with Fluorohub single photon counting. From the theoretical fitting data, we found that the average life time is 130 ns for only GCDs and 3.9 nm for GNP attached GCDs. The trend of the molecular excited-state lifetime for PD and GCDs as a function of its separation from 40 nm GNP is reported in Figure 3C. Reported distance dependent nanoparticle-induced lifetime also shows similar trend as we have observed for distance dependent quenching efficiency for PD and GCDs. The trend of the molecular excited-state lifetime for PD and GCDs as a function of its separation from 40 nm GNP is reported in Figure 3C. Reported distance dependent nanoparticle-induced lifetime also

shows similar trend as we have observed for distance dependent quenching efficiency for PD and GCDs. Since GCD exhibit small plasmon band around 520 nm, there will be strong plasmon coupling between GCD and GNP, which allows the softer dependence of the interaction strength on particle separation distance r. As a result, a much longer interaction range for GCD based NSET is expected compared to PD based NSET. Figure 3E show that the distance-dependent quenching efficiency between GCDs and GNP is highly dependent on the particle size. As reported in Figure 3E, the distance at which the energy transfer efficiency is 50% varies from 10 to 25 nm with the size of gold nanoparticles. Reported experimental data clearly show that gold nanoparticle size strongly affects the quenching efficiency and distance-dependent NSET behavior

A key advantage of our NSET system is that due to the large dimensions of GNP size, it allows conjugation with multiple types of donors directly to the surface of the nanoparticle. Figure 2E shows that the gold nanoparticle is able to quench the fluorescence from PD based ruler as well as GCD based ruler simultaneously. In this case, the gold nanoparticle acts both as a very efficient acceptor and as a sca□old which determines the spatial distribution of the donors. Experimental data as reported in Figure 3B show that the distance dependent quenching behavior for multicolor NSET is similar to single color NSET, as reported in Figure 3A. Reported experimental data indicate that cross-talk between two nanodots is minimum for the multicolor NSET probe developed by us and as a result, it can be used for accurate identification and quantification of multiple bio-molecules. Since it is now well documented that due to the tumor heterogeneity, cancer is the second leading cause of death for human being in our world [26-29]. To demonstrate the practical use for multicolor NSET ruler based probe for multiplex live cell detection, we have developed multicolor NSET by using DNA/RNA aptamer based ruler that are specific for the target cancer cells. Since Apt1 is known for specific to CD44 (+) cancer stem cells [31], for demonstrating targeted screening of breast cancer stem cells, we have used PD coated extended sequence of Apt1 (5′-GGGAUGGAUCCAAGCUUACUGGCAUCUGGAUUUGCGC GUGCCAGAAUAAAGAGUAUAACGUGUGAAUGGGAAG CUUCGAUAGGAAUUCGG**UCCAAGCUAG**-3′-PD, to target cancer stem cells, where the underlined sequence was the extended sequence, which has been used to develop the optical ruler.

In the next step, complementary sequences attached gold nanoparticles was mixed with PD coated Apt. 1 aptamer in 10 mM PBS solution containing 0.3 M NaCl, Excess PD/GCD coated aptamer which were not involved in hybridization were removed by centrifugation from the solution. In this NSET ruler, only underlined sequence of Apt. 1 will take part in NSET ruler formation and other portion will be free to bind with targeted cancer cells as shown in Figure 4A. Now in the presence of cancer stem cells, Apt. 1 will be exposed to cancer cell surface, and as a result, aptamers will fold in such a way that it will specifically bind to the target CD44 on cell surface as shown in Figure 4A. Due to the above fact, PD coated aptamer will be released from GNP and fluorescence signal from NSET probes will recover, as shown in Figure 4B. To demonstrate the targeted and simultaneous CSCs and epithelial cells imaging possibility, we have used CD44 (+) MDA-MB-231breast cancer stem cells and HER2 (+) SK-Br-3 epithelial breast cancer cells mixture. Since real life sample from cancer patients will contain several million peripheral blood mononuclear cells (PBMC) with cancer

cells, we have used PBMC cells for demonstrating the selectivity. S6 aptamer is known to be specific to human epidermal growth factor receptor 2 (HER2) [5,8], for demonstrating targeted screening of SK-BR-3 epithelial breast cancer cells, we have used GCD coated extended sequence of S6 aptamer[32] (5′TGGATGGGGAGATCCGTTGAGTAAGCGGGCGTGTCTC TCTGCCGCCTTGCTATGGGG **UACTUG**--3′), where the underlined sequence was the extended sequence, which has been used for the formation of optical ruler.

To understand whether PDs nanoprobe coated aptamers are bound to the CD44(+) cells after release from GNP, we have performed fluorescence mapping using an Olympus IX71 inverted confocal fluorescence microscope fitted with a SPOT Insight digital camera. For this purpose, at first, NSET probes were separated from cancer cells via centrifugation at 4500 rpm for 20 minutes and then thoroughly washed using buffer. Figure 3C shows the blue luminescence image of CD44(+)MDA-MB-231 cells, which clearly indicates that indeed the PDs nanoprobe attached aptamers are bound to the CSC surface, and as a result, we have observed blue color image.
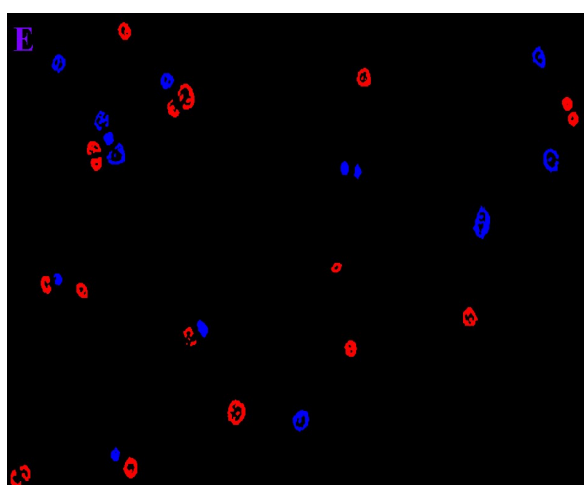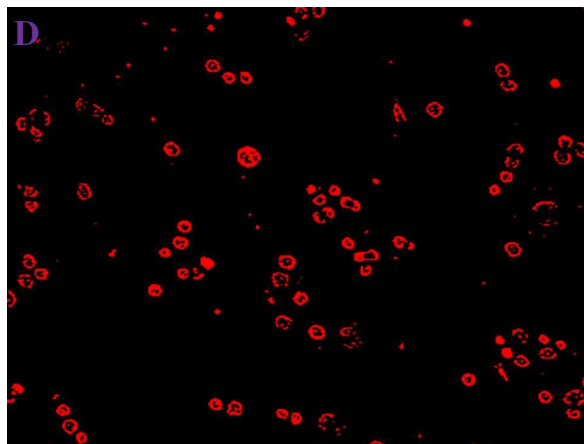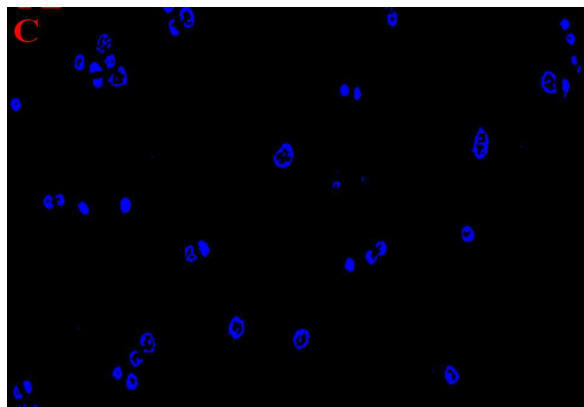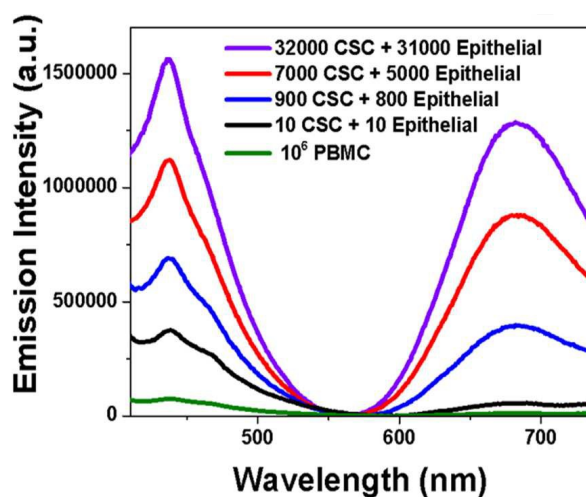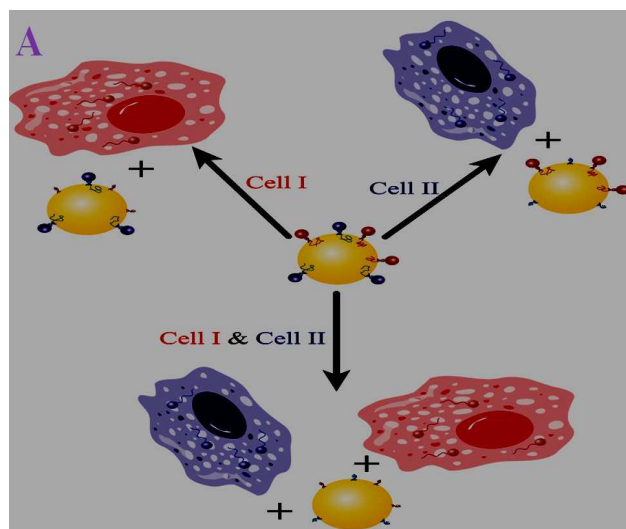

Figure 4: A) **Schematic representation shows the working principle of our multicolor NSET ruler based probe for screening of CD44 (+) CSC cell and HER2(+) SK-BR-3 cells simultaneously. B) Plot shows how** the **fluorescence intensity from PD coated Apt. 1 aptamer and GCD coated S6 aptamer varies in the presence of different numbers of CSC and SK-BR-3 cells together.. C) Single-photon luminescence image shows that PD coated Apt. 1 aptamers were bound on CD44 (+) CSC cell surface and as a result, we have observed blue fluorescence form CD44 (+) cells. D) Single-photon luminescence image shows that GCD coated S6 aptamers were bound to HER2 (+) SK-BR-3 cells surface, and as a result, we have observed red fluorescence form epithelial cells. E) Single-photon luminescence image shows using PD**

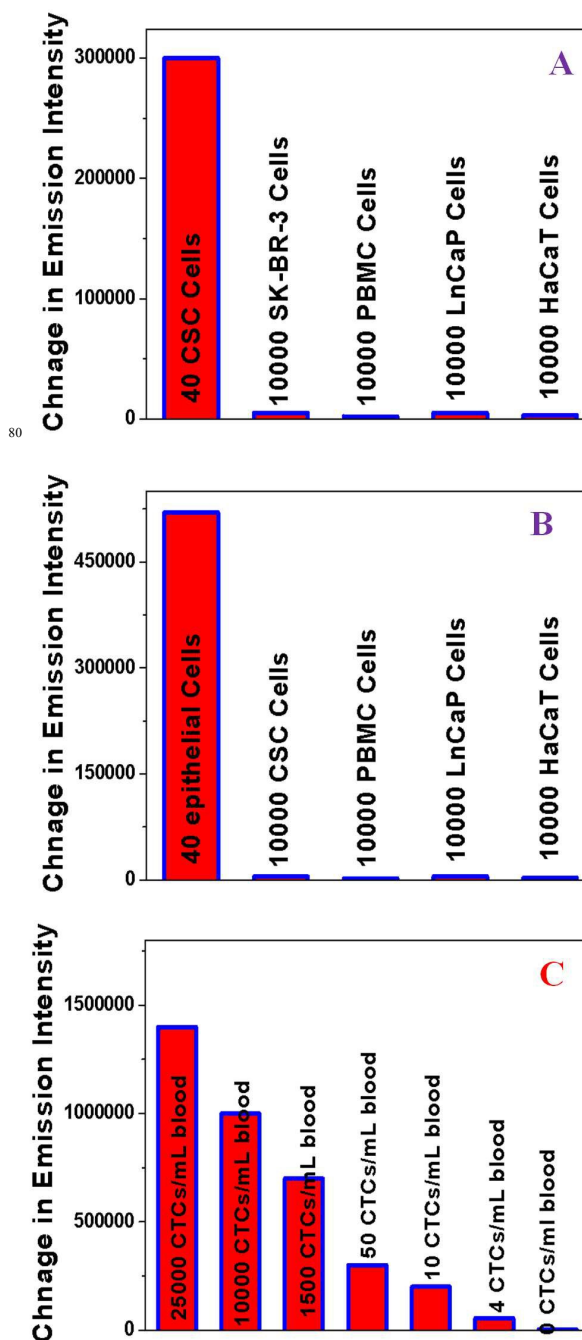**coated Apt. 1 aptamers and GCD coated S6 aptamer we can image epithelial and stem cells simultaneously.**

Similarly, Figure 3D shows the red luminescence image of HER2(+) SK-BR-3 cells, which clearly indicates that indeed the PDs nanoprobe attached aptamers are bound to the epithelial cell surface and as a result, we have observed red color image. The reported data clearly indicate that NSET probe is capable of screening CSC and epithelial cells.

To understand the selectivity of the NSET probe for the detection of CSC and epithelial cell, we have tested the selectivity with several other cell lines such as prostate cancer LnCaP cells, peripheral blood mononuclear cells (PBMC) and HaCaT normal skin cells. Figure 5A clearly shows that PD coated Apt. 1 aptamer based NSET probe is highly selective for CD44(+)CSC cells. As reported in Figure 5A, huge amount of fluorescence signal change even in the presence of 40 CD44(+) CSC cell, whereas we have not observed any fluorescence change even in the presence of 10^4 epithelial or 10^4 PBMC or other cells, which indicates that PD coated Apt. 1 aptamer based NSET probes are highly selective for targeted CSC cells. It can separate CSC cells from other cells lines such as epithelial, PBMC, LnCaP at HaCaT. On the other hand, as reported in Figure 5B, GCD coated S6 aptamers based NSET probe is highly selective for HER2 (+) SK-BR-3 epithelial cells. It can separate epithelial cells from other cells lines such as CSC, PBMC, LnCaP at HaCaT. Similarly Figure 4B shows that PD coated Apt. 1 aptamer and GCD coated S6 aptamers based NSET probes are highly selective for CSC and epithelial cell. It can separate epithelial & CCS cells from other cell lines easily. Figure 4B shows that the NSET probe can detect CSC and epithelial cells simultaneously, even at the concentration of 10 cells/mL blood, when 15 ml whole blood sample has been used.

As we have discussed before, several recent studies have demonstrated that blood sample in cancer patients will contain cancer epithelial cells and cancer stem cells together [1-10]. As a result, we have used our NSET probe for screening SK-BR-3 epithelial cancer cell and CD44+ CSC cells simultaneously from whole blood sample. For this purpose different concentrations of tumor cells and 10^6 cells/mL peripheral blood mononuclear cells (PBMC) were spiked into 15 mL suspensions of citrated whole blood purchased from Colorado Serum Company. Since in the clinical blood sample from patients, different tumor cells will coexist with the several million peripheral blood mononuclear cells, we have spiked 10^6 cells/mL peripheral blood mononuclear cells (PBMC) with cancer cells. In the next step, we have performed 90 minutes of gentle shaking. After that we have used the above spiked whole blood sample for our experiment. As shown in Figure 4B shows that in the presence of CD44 (+) cancer stem cells and HER2(+) epithelial cells together, we observed a very distinct fluorescence signal change in the blue and red zone simultaneously. On the other hand, no fluorescence signal change has been observed in the absence of CD44 (+) cancer stem cells and HER2(+) epithelial cells, when only 10^6 cells/mL peripheral blood mononuclear cells (PBMC) are present in whole blood sample. Figure 4E shows the presence of both, blue luminescence image of CD44(+)MDA-MB-231 cells and red luminescence image of HER2 (+) SK-BR-3 cells**.** Observed blue images are due to the PDs nanoprobe attached aptamers binding on the CSC surface and red luminescence images are due to the GCDs nanoprobe attached aptamers binding on the epithelial cells surface. The reported data clearly indicate that NSET probe

is capable of screening CSC and epithelial cell simultaneously from whole blood sample.

To understand the selectivity of the NSET probe for the detection of CSC and epithelial cell from whole blood sample, we have tested the selectivity with prostate cancer LnCaP cells and HaCaT normal skin cells. Figure 5D clearly shows that NSET probe is highly selective for CSC and epithelial cells. As reported in Figure 5D, huge amount of fluorescence signal change happens even in the presence of 30 CD44(+) CSC + 30 HER2(+) epithelial cells, whereas we have not observed any fluorescence change even in the presence of 10^4 HaCaT and LnCaP cells, which indicates that NSET probes are highly selective for targeted CSC and HER2(+) epithelial cells from whole blood sample.
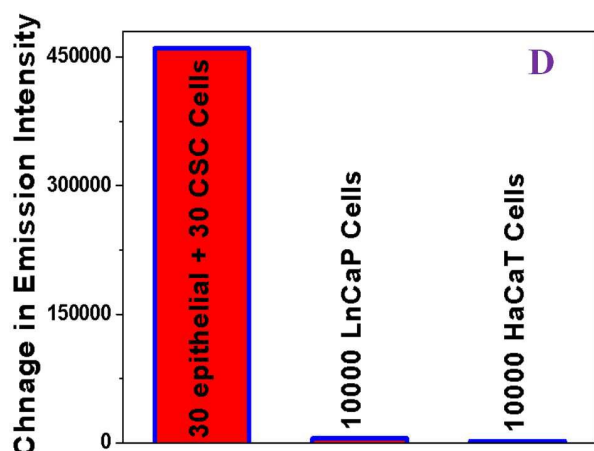
Figure 5: A) Plot shows the selectivity of PD coated Apt. 1 aptamer based NSET probe for the detection of CD44(+)CSC cells. B) Plot shows the selectivity of GCD coated S6 aptamers based NSET probe for the detection of HER2 (+) SK-BR-3 epithelial cells. C) Plot shows the detection efficiency of the NSET probe for the detection of CTCs from blood. We have used equal number of CSC and epithelial cells. Result shows that the detection efficiency is 4 CTCs/ml of blood, when 15 ml of infected whole blood has been used. D) Plot shows the selectivity of GCD coated S6 aptamers and PD coated A1 aptamer based NSET probe for the detection of CSC and epithelial cells.

Next, to understand the sensitivity of the NSET probe for the detection of CSC and epithelial cell from whole blood sample, we have tested blood sample infected by different amount of CTCs. We have used equal number of CSC and epithelial cells. Reported results in Figure 5C clearly shows that that the detection efficiency is 4 CTCs/ml of blood, when 15 ml of infected whole blood has been used.

Conclusion

In conclusion, in this article we have reported the development of long-range multi color nanoscopic ruler using blue color fluorescence polymer dots and red color fluorescence gold cluster dots as donors and 40 nm gold nanoparticle as an acceptor. We have demonstrated that the multicolor NSET probes are capable of selective and simultaneous detection of CD44(+) CSCs and HER2(+) epithelial cells. Our reported experimental data demonstrated that the multicolor nanoscopic ruler's working window is above 35 nm distance, which is more than three times farther than that of FRET detection limit. Theoretical modeling using Förster dipole−dipole coupling and NSET based dipole-to-nanoparticle surface energy transfer indicate that the observed experimental long distance quenching rate cannot be discussed using the classical $1/R^6$ characteristic of FRET. On the other hand, good agreement between experimental data with NSET model has been achieved when polymer dots acts as a donor and GNP as an acceptor. Reported data also indicate that the agreement is quite poor with NSET model when gold cluster dots act as a donor and GNP acts as an acceptor. Our reported data using non-targeted peripheral blood mononuclear cells (PBMC) and normal skin HaCaT cells show that developed nanoscopic ruler based probes are highly selective for capturing targeted tumor cells. We have shown that NSET probe based multicolor fluorescence imaging can be used for mapping epithelial and stem cells simultaneously from blood sample. After proper engineering design, reported nanoscopic rulers will be capable of finding tumor heterogeneity by accurately identifying CSCs and epithelial cells from clinical sample in clinics.

Experimental

We have purchased branched polyethyleneimine polyvinyl alcohol, gold chloride, D,L-Lactide, sodium borohydride, sodium acetate, and 1,6-hexadiamine and all other reagents and solvents from Sigma-Aldrich (St. Louis, MO, USA). All aptamers were purchased from Midland Certified Reagent All epithelial, stem and normal cell lines were purchased from the American Type Culture Collection (ATCC, Rockville, MD).

Synthesis of blue fluorescence polymer dots (PDs): Blue fluorescence polymer dots (PDs) were synthesised using amphiphilic polymer solvent evaporation technique [17]. Initially we have synthesized polyethyleneimine and hydrophobic polylactide (PEI-PLA) Copolymer. For this purpose, 15 g of pre-dehydrated D,L-lactide was dissolved in 50mL of anhydrous dimethysulfoxide solvent and on that 0.5g of PEI and 0.05M trimethylamine was added. We have kept the mixture under nitrogen at 86°C for 12 hours under gentle stirring. After that the solution was poured on ice cold water and then precipitate was collected which was thoroughly washed with nanopure water. In the next step, 20 mg of PEI-PLA copolymer was dissolved in 2mL of dichloromethane and 1% (w/v) of PVA. The mixture was kept at 35°C in vacuum chamber to let the dichloromethane evaporate. To purify the product we have centrifuged at 1500 rpm for 20 minutes. The purified particles were characterized by high-resolution SEM as reported in Figure 6B, which clearly shows that the size is about 4-5 nm. To measure the size, zeta potential and polydispersity of freshly prepared polymer dots, we used Malvern Zetasizer Nano instrument. Inserted histogram in Figure 6B shows the size distribution for polymer dots which indicate that the size is about 4 ± 2 nm. Zeta potential for the polymer dots was determined to be −26.19 mV. The emission spectra, as reported in Figure 6D, clearly shows that the λ_{max} for emission for PDs coated aptamers is around 440 nm and as a result, it shows blue color fluorescence. The photoluminescence quantum yield (QY) for PD was determined to be 0.69 at 380 nm light excitation, using quinine sulfate as a standard (QY 54%).

Development of PDs coated Apt. 1 aptamer: For targeted capture and imaging of CD44(+) CSCs, blue fluorescence PDs nanoprobe were attached with Apt. 1 aptamer which known to be specific for CD44(+). To accomplish this, amine modified Apt. 1aptamer was used. We have used EDC/NHS esterification for the conjugation between amine group of amine modified aptamer and -OH group of polymer dots.

Synthesis of red fluorescence GNCs: Red fluorescence GCDs nanoprobes were synthesized using a multistep process [29]. For this purpose initially, 0.2ml Sodium hydroxide (2M) was mixed with α-Lipoic acid (10.0 μM) at room temperature under vigorous stirring. In the next step, 0.8ml of $HAuCl_4.3H_2O$ was added drop wise to the mixture and then we have added 800 micro liter of 100mM $NaBH_4$ with constant stirring. Resulting GCDs products were purified by centrifugation at 7500 rpm for 45 minutes using a filter with 3,000 MWCO. The purified particles were characterized by high-resolution TEM, as reported in Figure 6C, which clearly shows that the size is about 3-4 nm. Inserted

histogram in Figure 6C shows the size distribution for gold dots which indicate that the size is about 3 ± 2 nm. Zeta potential for the gold dots was determined to be −14.6 mV. Figure 5E shows the red emitted fluorescence from GCD in the presence of UV
5 light. Reported emission spectra clearly show that the λ_{max} for emission for GCDs coated aptamers is around 680 nm and as a result, it shows red color fluorescence. The photoluminescence quantum yield (QY) for GCD was determined to be 0.13 at 380 nm light excitation, using quinine sulfate as a standard (QY
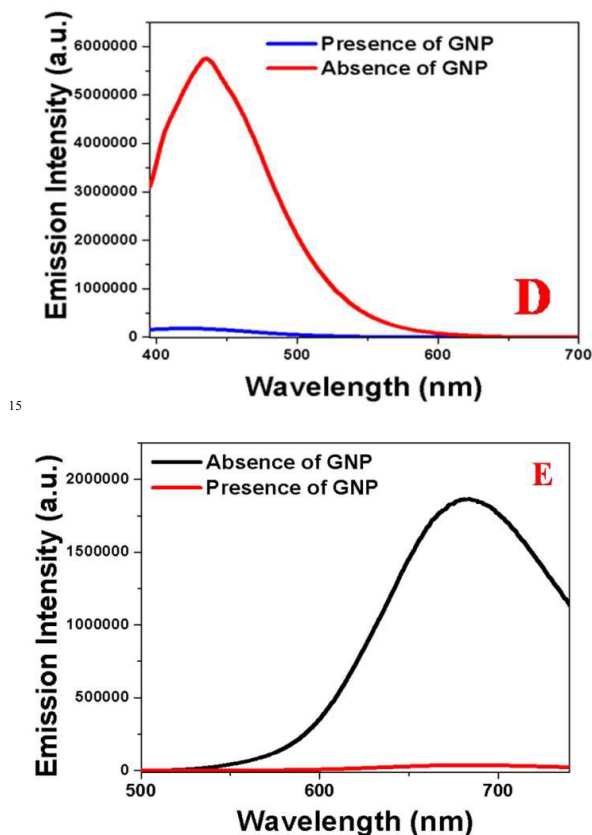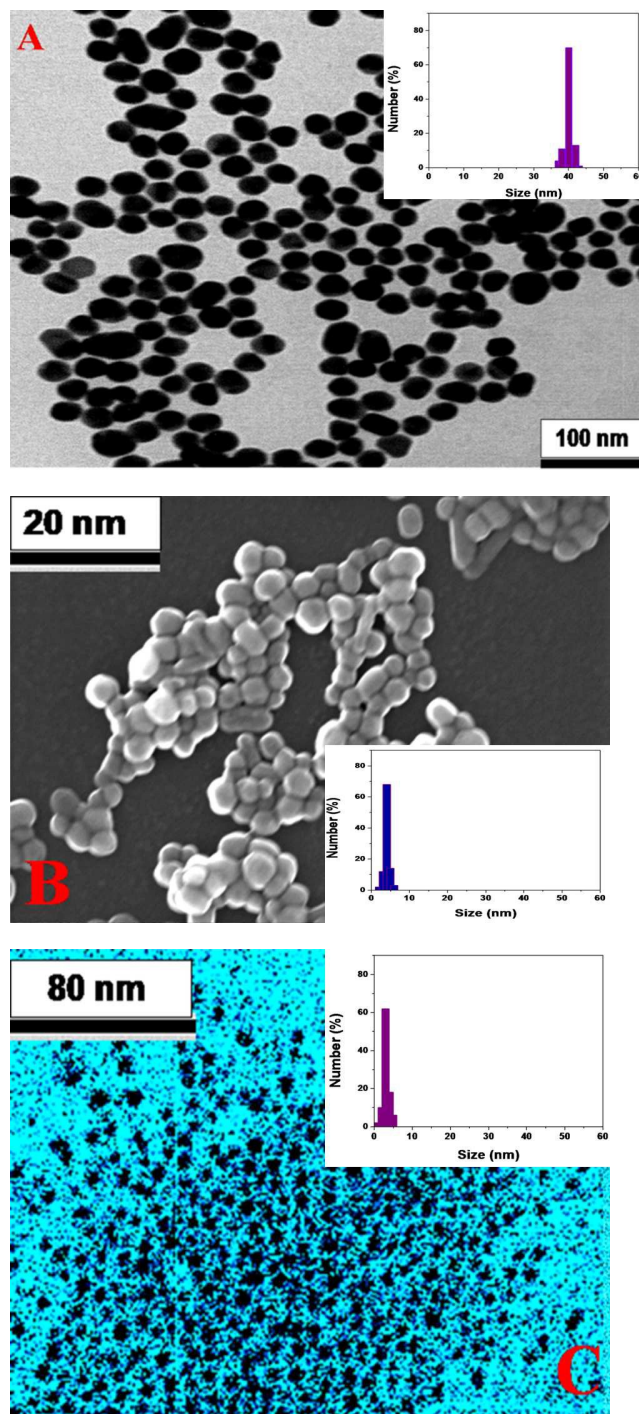10 54%).

15

Figure 6: A) TEM image shows the morphology of freshly prepared gold nanoparticles, whose size is about 40 nm. Inserted histogram shows the size distribution for gold
20 nanoparticles which indicate that the size is about 40 ± 5 nm. **B)** SEM image shows the morphology of freshly prepared polymer dots (PDs), whose size is about 4 nm. Inserted histogram shows the size distribution for polymer dots which indicate that the size is about 4 ± 2 nm. **C)** TEM image shows
25 the morphology of freshly prepared gold cluster dots, whose size is about 3 nm. Inserted histogram shows the size distribution for gold dots which indicate that the size is about 3 ± 2 nm. **D)** Fluorescence spectra from 5′-polymer dots modified oligonucleotides (6 mers) in the presence and
30 absence of gold nanoparticle. **E)** Fluorescence spectra from 5′-gold cluster dots modified oligonucleotides (6 mers) in the presence and absence of gold nanoparticle.

Development of GCDs coated S6 aptamer: For targeted capture
35 and imaging of HER2(+) epithelial cells, red fluorescence GCDs nanoprobe were attached with S6 aptamer which known to be specific for HER2(+). To accomplish this, amine modified S6 aptamer was used. For this purpose, we have used coupling chemistry between -CO_2H group of α-Lipoic acid attached
40 GCDs and -NH_2 group of amine-functionalized S6 aptamer via amide linkages in the presence of 1-(3-dimethyl-aminopropyl)-3-ethylcarbodiimide hydrochloride (EDC).

Synthesis of gold nanoparticle: Gold nanoparticles around nm
45 in size were synthesized by using 0.01 wt.% chlorauric acid ($HAuCl_4$) and 1 wt.% trisodium citrate dehydrate, as reported by our groups before [11,13,14]. After that spherical gold nanoparticles were characterized using TEM, as reported in Figure 6A, which indicates that the size is about 40 nm. To
50 measure the size, zeta potential and polydispersity of freshly

prepared gold nanoparticle, we used Malvern Zetasizer Nano Inserted histogram in Figure 6A shows the size distribution for gold nanoparticles which indicate that the size is about 40 ± 5 nm. Zeta potential for the spherical gold nanoparticle was determined to be −6.84 mV.

Development of nanoscopic ruler: To design long-range multicolor nanoscopic rulers of different lengths, we used 5′-PD/GCS- and 3′-SH modified ssRNA of different lengths. After hybridization with complementary oligonucleotides, the separation distances between the GNP and PD/GCD nanodots were systematically varied. For this purpose, we have used the captured oligonucleotides from 2 mer to 130 mer. Some of the oligonucleotides structure is shown below.

2mer: 5′-GG-3′-SH
18mer: 5′-GGG AUG GAU CCA AGC UUA -3′-SH
36mer: 5′-GGG AUG GAU CCA AGC UUA CUG GCA UCU GGA UUU GCG -3′-SH
63mer: 5′-GGG AUG GAU CCA AGC UUA CUG GCA UCU GGA UUU GCG CGU GCC AGA AUA AAG AGU AUA ACG UGU -3′SH
130mer: 5′-GGG AUG GAU CCA AGC UUA CUG GCA UCU GGA UUU GCG CGU GCC AGA AUA AAG AGU AUA ACG UGU GAA UGG GAA GCU UCG AUA GGA AUU CGG UCU GGA UUU GCG CGU GCC GGG AUG GAU CCA AGC UUA CUG G-3′SH

In our design, we have estimated the "multicolor NSET ruler" distance using the simple model reported by Clegg et al. [45], by taking into account the size of the 0.32 nm for each base pair. We have also used 2.8 nm for Au–S-$(CH_2)_n$-RNA and RNA-PD distance in both sides of base pair. To find out the validity of rigid-rod approximation we have used dynamic light scattering (DLS) measurement using a Malvern Zetasizer Nano instrument. We have reported before that DLS can be used to measure the distance between GNP and dye, when they are separated by –ds DNA/RNA[11,14]. Table 1 clearly shows that that the DLS measurement data are quite close to our estimated distances using rigid-rod approximation.

Cell culture: CD44 (+) MDA-MB-231breast cancer cells and HER2 (+) SK-Br-3 epithelial breast cancer cells, CD44(-) and HER2(-) Human normal skin HaCaT cell lines were purchased from the American Type Culture Collection (ATCC) . We have grown all those cells according to the ATCC procedure. Once the cultured cells was more than 10^6 cells/mL, different numbers of individual or mixture of epithelial and CSCs were spiked in citrated whole rabbit blood at various densities for screening experiment**.** Using an enzyme-linked immunosorbent assay kit, the measured amount of HER2 in SK-BR-3 cells was 4.1 × 10^6/cell. No HER2 was found in PBMC, MDA-MB-231 and HaCaT cells. Similarly, using an enzyme-linked immunosorbent assay kit, the measured amount of CD44 in MDA-MB-231 cells was 5.6 × 10^5/cell. No CD44 was found in PBMC, SK-BR-3 or HaCaT cells

Fluorescence mapping of epithelial and CSCs: For the fluorescence imaging of epithelial and CSCs selectively and simultaneously an Olympus IX71 inverted confocal fluorescence microscope fitted with a SPOT Insight digital camera was used.

LIVE SUBJECT STATEMENT:

All cell line experiments were performed in compliance with the relevant laws and institutional guidelines. Jackson State University's institutional review board (IRB00001419) has approved the experiments and we have IRB approval for human subjects research till October 2016.

Acknowledgements

Notes and References

1. 1. M. S. Sosa, P. Bragado, J. A. Aguirre-Ghiso , *Nat Rev Cancer.* 2014, **14**, 611.
2. L. Chang, J. Hu, F. Chen, Z. Chen, J. Shi, Z. Yang, Y. Li and L. J. Lee , *Nanoscale*, 2016, **8**, 3181-3206
3. A. Marusyk, V. Almendro, & K. Polyak, K. *Nature Rev. Cancer* 2012, **12**, 323.
4. 4. R. M. Mohamadi, J. D. Besant, A. Mepham, B. Green, L. Mahmoudian, T. Gibbs, I. Ivanov, A. Malvea, J. Stojcic, A. L. Allan, L. E. Lowes, E. H. Sargent, R. K. Nam, and S. O. Kelley, *Angew. Chem. Int. Ed.* 2015, **54**, 141.
5. B. P. V. Nellore, R. Kanchanapally, A. Pramanik, S. S. Sinha, S. R. Chavva, A. Hamme, and P. C. Ray, P. C. *Bioconjugate Chem.*, 2015, **26**, 235–242.
6. S. Wang, K. Liu, J. Liu, T. F. Yu, X. Xu, L. Zhao, T. Lee, K. E. Lee, J. Reiss, Y. K. Lee, L. W. K. Chung, J. Huang, M. Rettig, D. Seligson, K. N. Duraiswamy, C. K. F. Shen, H. R. Tseng, *Angew. Chem., Int. Ed.* 2011, **50**,3084–3088
7. Y. Zhang Y, M. Wu, X. Han , P. Wang, L. Qin, *Angew. Chem. Int. Ed.* 2015, **54**, 10638.
8. Z. Fan, M. Shelton, A. K. Singh, D. Senapati, S. A. Khan and P. C. Ray, P. C. *ACS Nano*, 2012, **6**,1075.
9. Xingsheng Xu and Huayong Wang *Nanoscale*, 2016,**8**, 342-347
10. L. Yan, Y. Zhang, B. Xu and W. Tian , *Nanoscale*, 2016,**8**, 2471-248
11. P. C. Ray, Z. Fan,; R. A. Crouch,S. S. Sinha, A, Pramanik, A. *Chem. Soc. Rev.* 2014, **43**, 6370.
12. C.Yun, A. Javier, T. Jennings, M. Fisher, S. Hira, S. Peterson, B. Hopkins, N. O. Reich, G. F. Strouse, *J. Am. Chem. Soc.*, 2005**, 127**, 3115.
13. J.Griffin, A.K. Singh, D.Senapati, P. Rhodes, K. Mitchell, B. Robinson, E. Yu, P.C. Ray, *Chem. - Eur. J.* 2009, **15**, 342.
14. A. K. Singh, S. A. Khan, Z. Fan, T. Demeritte, D. Senapati, R. Kanchanapally and P. C. Ray, *J. Am. Chem. Soc.* 2012, **134**, 8662-8669
15. R. A. Riskowski, R. E. Armstrong, N. L. Greenbaum, and G. F. Strouse, *ACS Nano*, 2016, Article ASAP
16. S. T. Kochuveedu and D. H. Kim , *Nanoscale*, 2014,**6**, 4966-4984
17. Y. Sun, W. Cao, S. Li, S. Jin, K. Hu, K.; *et al. Sci. Rep.,* 2013, **3**, 3036
18. A. Pramanick, Z. Fan, S. R. Chavva, S. S. Sinha, P. C. Ray, *Sci Rep* 2014, **4**, 6090.
19. J. Liu, N. P. Wickramaratne, S.Z. Qiao, M. Jaroniec, M. *Nat. Mater.* 2015, **14**, 763.
20. Y. A. Shi, A. Pramanik, C. Tchounwou, F. Pedraza, R .A. Crouch, S. R. Chavva, A. Vangara, S. S. Sinha, S. Jones, D. Sardar, C. Hawker, and P. C. Ray, *Appl. Mater. Interfaces* 2015, **7,** 10935.

21. L. Guo, J. Ge, W. Liu, G. Niu, Q. Jia, H. Wang and P. Wang , *Nanoscale*, 2016,**8**, 729-734

22. S. Wang, X. Meng, A. Das, T. Li, Y. Song, T. Cao, X. Zhu, M. Zhu and R. Jin, *Angew Chem Int Ed.* 2014, **53**, 2376.

23. K. Jiang, S. Sun, L. Zhang, Y. Lu, A. Wu, C. Cai, H. Lin, *Angew. Chem., Int. Ed,* 2015**,** *54*, 5450-5453

24. S. E. Crawford, C. M. Andolina, A. M. Smith, A. M.; Marbella, L. E.; Johnston, K. A.; Straney, P. J.; Hartmann, M. J.; and J Millstone, J. E.; *J. Am. Chem. Soc.*, 2015, **137**, 14423–14429.

25. Zhang, X. X. Yang, Y. Wang, N. W. Zhao, Z. H. Xiong and C. Z. Huang , *Nanoscale*, 2014,**6**, 2261-2269.

26. Das, A.; Li, T.; Nobusada, K.; Zeng, Q.; Rosi, N. L.; Jin, R. *J. Am. Chem. Soc***.** 2012, *134*, 20286–20289..

27. A. K. Singh, R. Kanchanapally R, Fan Z, Senapati D, P. C. Ray, *Chem. Commun.* 2012**, 48**, 9047– 9049.

28. S. Chen, S. Wang, J. Zhong, Y. Song, J. Zhang, H. Sheng, Y. Pei and M. Zhu, *Angew. Chem., Int. Ed,* 2015**,** *54*, 3145.

29. L. Shang, N. Azadfar N, Stockmar F, Send W, Trouillet V, Bruns M, Gerthsen D, Nienhaus GU. , *Small*, 2011, **7**, 2614-2620.

30. Clegg, R.M.; Murchie, A.I.H.; Zechel, A.; Lilley, D. M. J. *Proc. Natl. Acad. Sci. U.S.A.* 1993, **90**, 2994–2998.

31. Y. Zhang, M. Wu, X. Han , P. Wang, L. Qin, *Angew. Chem. Int. Ed*. 2015, **54**, 10638

32. S. H. King, Y. M. Huh, S. Kim, D. K. Lee, *Bull. Korean Chem. Soc.* 2009, **30**,1827